Tailoring the light-matter coupling in anisotropic microcavities: Redistribution of oscillator strength in strained *m*-plane GaN/AlGaN quantum wells

G. Rossbach,* J. Levrat, A. Dussaigne,† G. Cosendey, M. Glauser, M. Cobet, R. Butté, and N. Grandjean
Institute of Condensed Matter Physics, École Polytechnique Fédérale de Lausanne, CH-1015 Lausanne, Switzerland

H. Teisseyre
Institute of High Pressure Physics, Polish Academy of Sciences, PL-01-142 Warsaw, Poland and
Institute of Physics, Polish Academy of Sciences, PL-02-668 Warsaw, Poland

M. Bockowski, I. Grzegory, and T. Suski
Institute of High Pressure Physics, Polish Academy of Sciences, PL-01-142 Warsaw, Poland
(Received 19 May 2011; published 21 September 2011)

We present a comprehensive study of the anisotropic optical properties of nonpolar GaN/AlGaN multiple quantum wells intentionally designed to act as an active region of a planar microcavity operating in the strong-coupling regime. The strain induced by the underlying AlGaN-based Bragg reflector leads to a redistribution of exciton oscillator strength as revealed by photoluminescence and reflectivity measurements. Complementary $k \cdot p$ calculations show an excellent agreement with experiments and emphasize the opportunity to tune the nature of the light-matter coupling in a microcavity by means of strain engineering. Finally, the validity of the developed model is proven by angle-resolved photoluminescence studies carried out on the complete microcavity structure. The recorded eigenmode spectra reveal the coexistence of the weak- and the strong-coupling regime along the two orthogonal polarization planes.

DOI: 10.1103/PhysRevB.84.115315 PACS number(s): 78.67.De, 78.55.Cr, 78.40.Fy, 78.20.Fm

I. INTRODUCTION

The hexagonal symmetry of the wurtzite lattice, the thermodynamically stable crystal structure of common III nitrides, causes uniaxial anisotropy of many material properties and, in combination with the ionic bonding between nitrogen and metal atoms, an intrinsic polarization along the [0001] direction (c axis). Heterostructures grown along this polar orientation, e.g., quantum wells (QWs), experience the so-called quantum-confined Stark effect (QCSE): A built-in electric field issued from the polarization discontinuity at the interfaces, which might be additionally modified by a strain-induced piezoelectric component, separates electron and hole wave functions toward opposite sides of the well.[1] Hence, the wave-function overlap and therefore the oscillator strength (f_{osc}) decrease, and the overall efficiency of such QW-based devices is reduced.

In order to circumvent these drawbacks the growth of nonpolar III-nitride heterostructures with $(10\bar{1}0)/m$-plane or $(11\bar{2}0)/a$-plane surface orientation is of large interest.[2] They are no longer subject to the QCSE, but exhibit a pronounced anisotropic optical response governed by birefringence and dichroism—two effects arising from the uniaxial character of the complex refractive index tensor. Birefringence is related to the real part: Light propagation with the electric field vector $\mathbf{E}$ polarized perpendicular and parallel to the c axis, namely, in the ordinary and extraordinary direction, is governed by different refractive indices n_o and n_e (indices o and e denote the ordinary and extraordinary directions, respectively). By contrast, dichroism is created by different imaginary parts for the two polarization directions. It relies on the symmetry of the bands involved in the optical transitions near the band edge. Since the response of the s-orbital-like conduction band (Γ_7^c) is almost isotropic, the selection rules are primarily generated by the symmetry of the three valence bands (Γ_9^v, Γ_{7+}^v, and Γ_{7-}^v symmetry in order of decreasing energy; the corresponding transitions are labeled as A, B, and C in the following). In the case of relaxed nonpolar GaN, the lowest-energy transitions A and B dominate the optical response for the ordinary direction $\mathbf{E} \perp c$ ($f_{\mathrm{osc},o}^{\mathrm{A}} : f_{\mathrm{osc},e}^{\mathrm{A}} = 0.5 : 0$, $f_{\mathrm{osc},o}^{\mathrm{B}} : f_{\mathrm{osc},e}^{\mathrm{B}} = 0.44 : 0.12$), while C rules the extraordinary one $\mathbf{E} \parallel c$ ($f_{\mathrm{osc},o}^{\mathrm{C}} : f_{\mathrm{osc},e}^{\mathrm{C}} = 0.06 : 0.88$).[3,4]

The nonpolar GaN-based multiple QW (MQW) structure investigated in this paper is intentionally designed to act as an active region of a planar microcavity (MC) operating in the strong-coupling regime (SCR).[5] In such MCs the coupling strength between the cavity mode C and the excitonic resonance X overcomes their damping rates and switches the system to a nonperturbative regime, where the new eigenstates are exciton polaritons combining characteristics of matter and light.[6] These structures are seen as promising candidates for future low-threshold coherent light emitters such as polariton lasers.[7–9] The magnitude of the coupling strength g depends, among others, on f_{osc}, the effective refractive index of the cavity n_C and the reflectivity of the cavity mirrors, which directly leads to polarization-dependent g values in optically anisotropic MCs.[10] Taking into account the strong dependence of f_{osc} on the strain state in III-nitride layers,[11] this fact suggests the possibility to tailor the light-matter coupling regime through strain engineering in such structures.

In this paper, we will first characterize the anisotropic optical response of a high-quality m-plane GaN/AlGaN MQW structure grown on top of a 50-pair $Al_{0.15}Ga_{0.85}N/Al_{0.35}Ga_{0.65}N$ distributed Bragg reflector

(DBR) by means of polarization-resolved photoluminescence (PL) and reflectivity measurements. Besides the expected polarization-dependent DBR stopband shift, we will show that the strain induced by the pseudomorphic growth of the MQW structure on the bottom DBR leads to a significant redistribution of f_{osc} in the vicinity of the band edge. Using $k \cdot p$ simulations, which agree well with optical measurements, we will emphasize an original way to tune the coupling strength in a full MC by adjusting the aluminum content in the bottom DBR bilayers. In the last section photoluminescence eigenmode spectra of the complete MC structure confirm the predictions from theoretical modeling and highlight a unique anisotropic coupling regime.

II. SAMPLE STRUCTURE AND EXPERIMENTAL DETAILS

For the achievement of high crystal and optical quality, the choice of the substrate is of primary importance. With the use of a 100-μm-thick m-plane bulk GaN substrate, lattice mismatch and differences in the thermal expansion coefficients are minimized, and the dislocation density is reduced (2×10^6 cm^{-2} in the substrate). The growth performed by molecular beam epitaxy using ammonia as a nitrogen source started with the deposition of a 400-nm-thick homoepitaxial GaN layer. Subsequently, a 50-pair $Al_{0.15}Ga_{0.85}N/Al_{0.35}Ga_{0.65}N$ DBR with nominal layer thicknesses of 31.8 and 34.8 nm, respectively, was grown. The overgrown MQW section, aimed at being the active region of the MC, consists of five QW sets located at the antinodes of the 3λ cavity, each being separated by 30.8 nm of $Al_{0.13}Ga_{0.87}N$. Each set is formed by four 5-nm-thick GaN QWs with 5-nm-thick $Al_{0.13}Ga_{0.87}N$ barriers. This region is surrounded by two $Al_{0.13}Ga_{0.87}N$ spacer layers with a thickness of 48.3 nm. Finally, the MC was completed by an eight-pair SiO_2/ZrO_2 dielectric top DBR deposited by the electron beam evaporation technique.

Cross-section scanning electron microscopy (SEM) images of the half MC (without top DBR) are shown in Fig. 1. The pairs of the AlGaN-based DBRs are clearly visible, evidencing smooth interfaces and a significant contrast created by the different Al contents. On top of the DBR the cavity region containing the five QW sections is well resolved.

PL studies were carried out using as an excitation source either a continuous wave (cw) frequency-doubled Ar-ion laser ($\lambda = 244$ nm) with an excitation power density of 2 kW/cm^2 or a pulsed frequency-quadrupled Nd:yttrium aluminum garnet (YAG) laser ($\lambda = 266$ nm), providing a pulse length of 500 ps, a repetition rate of 8.52 kHz, and a peak power density of 65 kW/cm^2. A microscope objective with a numerical aperture of 0.55 was used for the micro-PL measurements, where the spot diameter is $\sim$0.5 μm. Polarization-resolved PL studies were performed using a linear polarizer under collection normal to the sample surface and excitation under a fixed angle of 45°. The spot diameter in this configuration amounts to $\sim$50 μm and the angular resolution is better than 1°. The latter is also valid for reflectivity measurements, where a 150-W Xe lamp acted as the light source. The signal was collected through an optical fiber coupled to a liquid-nitrogen cooled UV-enhanced charge-coupled device monochromator combination, providing a spectral resolution of $\sim$100 μeV. A continuous-flow liquid-helium cryostat allowed tuning the temperature from 4 to 300 K. The eigenmode dispersion of the full MC was directly recorded by means of a Fourier imaging technique (far-field emission) using the microscope objective and pulsed excitation. With a spot size of $\sim$3 μm the peak power density amounts to 230 kW/cm^2 in this case. Polarization selection was achieved by a $\lambda/2$ waveplate in combination with a linear polarizer.

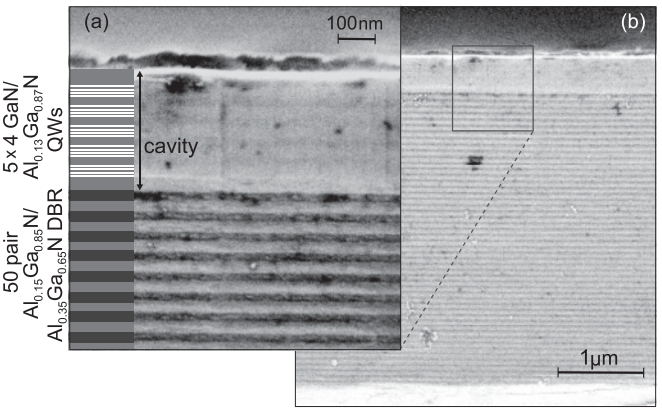

FIG. 1. Sample structure: (a) Enlarged cross-section SEM image of the cavity section deposited on top of a 50-pair AlGaN-based DBR, including a schematic sketch of the corresponding layer stack on the left-hand side. (b) Cross-section SEM view of the whole structure.

III. INVESTIGATIONS ON THE HALF MICROCAVITY

Figure 2 shows temperature-dependent micro-PL spectra taken under cw excitation without polarization selection. The emission from the QWs and the AlGaN -barriers can be easily followed up to room temperature (RT). At low temperatures both transitions show an additional emission from defect states $\sim$45 meV below the main transition, which might be

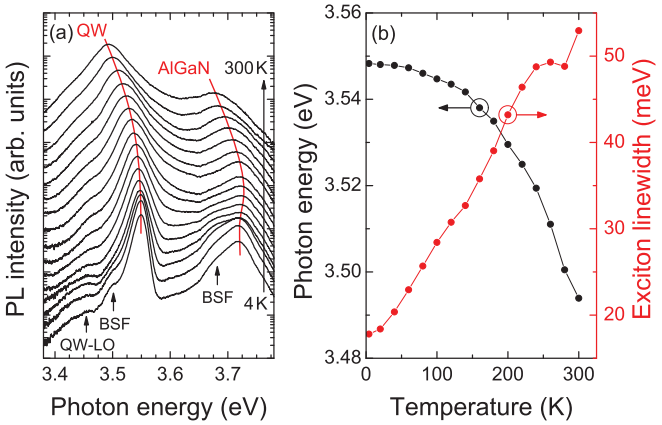

FIG. 2. (Color online) (a) Temperature dependent micro-PL spectra obtained under cw excitation (spectra are vertically shifted for the sake of clarity). The two red (gray) lines are a guide to the eye for the main emission peaks issued from the QW exciton and the AlGaN barrier. (b) Peak energy and linewidth of the QW emission as a function of temperature.

related to basal stacking faults (BSFs), a feature frequently observed in nonpolar III-nitride structures.[12] This emission is unpolarized and vanishes rapidly with increasing temperature, while the first longitudinal-optical phonon replica of the QWs (QW-LO) is well resolved for all temperatures. The QW peak energy exhibits a redshift of 55 meV from 4 to 300 K and a marginal signature of localization—contrary to the emission of the AlGaN barrier, emphasizing the strong impact of alloy fluctuations. Due to the absence of QCSE and the large QW width, the influence of the barrier disorder on the QW exciton is reduced, resulting in a shallower localization potential in the QW. Hence, considering the excitation power density, we assume almost all localization centers to be saturated, which leads to an emission dominated by free excitons. Nevertheless, the slightly asymmetric peak shape of the QW emission at low temperatures indicates the presence of localized states in its low-energy tail.

It is worth mentioning that the high quality of the QWs is confirmed by a narrow linewidth of ∼18 meV at 4 K and 53 meV at RT, which should be suitable for SCR studies. Indeed, in a previous study it has been shown that an inhomogeneous broadening γ_{inh} comparable to the value of the vacuum Rabi splitting Ω_{VRS} [cf. Eq. (3) hereafter] will inevitably lead to the loss of the SCR.[13] Considering the low-temperature linewidth as an upper limit for γ_{inh}, and assuming $\Omega_{\mathrm{VRS}} \sim 40$ meV (cf. Sec. V), the possibility to reach the SCR in this structure is clearly preserved.

To understand the optical behavior of such nonpolar quantum structures, polarization-resolved measurements are of major interest. Corresponding PL spectra acquired under pulsed excitation at 4 and 300 K are shown in Figs. 3(a) and 3(b), respectively. RT spectra are dominated by the QW emission, exhibiting a pronounced polarization dependence in intensity and peak energy [cf. Fig. 3(d)]. The anticorrelation between both quantities is remarkable: The highest PL peak intensity I appears for the lowest peak energy along the extraordinary direction and vice versa along the ordinary one. The relative energy shift ΔE amounts to ∼10 meV. This behavior is a clear indication of the existence of (at least) two exciton levels separated in energy by less than the linewidth and featuring an orthogonal polarization behavior. Their relative weight is determined by the thermal occupation and the distribution of f_{osc}. Note that ΔE corresponds to the lower limit of the level splitting, the former becoming valid for a linear polarization degree ($\rho = [I_{\mathbf{E}\parallel c} - I_{\mathbf{E}\perp c}]/[I_{\mathbf{E}\parallel c} + I_{\mathbf{E}\perp c}]$) equal to unity. According to the electronic properties of GaN we assign these two levels to the A and the B exciton in the following (X_{A} and X_{B}, respectively).[14] By contrast, at low temperature two additional features are well resolved [Fig. 3(a)]: the emission from the AlGaN barrier and the one from the homoepitaxial GaN buffer layer. The QW emission keeps the same polarization state over the whole temperature range and is copolarized with the barrier PL signal and counterpolarized with respect to the emission of the GaN buffer (maximum I for $\mathbf{E}\perp c$). For the QW and the buffer emission ρ was derived to be equal to 0.39 and −0.85, respectively. Compared with RT spectra the maximum intensity of the QW emission corresponds to the highest peak energy at 4 K. Here, two effects have to be considered. First, at this temperature the thermal occupation and therefore the influence of X_{B} is expected to be negligible. Furthermore, the PL contribution of localized states present in the low-energy tail of the QW emission has to be taken into account at low temperatures. Since they are expected to be unpolarized,[15] their influence increases in the polarization direction where the free exciton emission is minimal. As a result, the superposition of PL from localized and free excitons appears at lower energies. From polarization- and temperature-dependent studies we infer a QW localization energy between 10 and 15 meV.

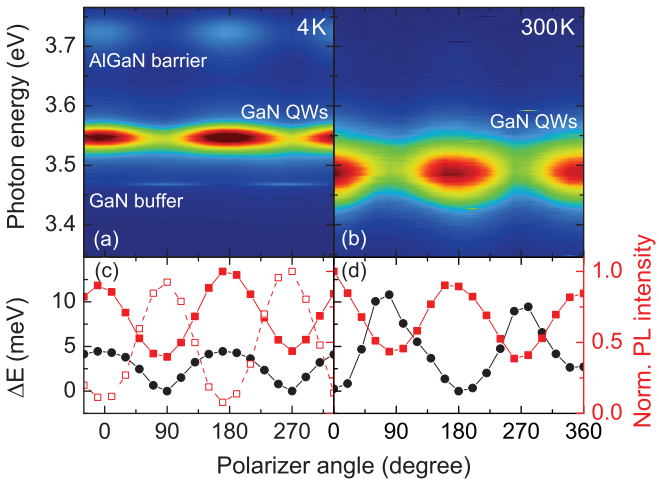

FIG. 3. (Color online) Color map of polarization-resolved PL spectra obtained under pulsed excitation at (a) 4 K and (b) 300 K. The relative evolutions of peak energy (black circles) and intensity (red solid squares) of the QW emission are shown in the bottom row: (c) at 4 K and (d) at 300 K. In (c) the intensity of the GaN buffer emission is also shown (red open squares). Polarization $\mathbf{E}\parallel c$ always corresponds to a polarizer angle of 0°.

This interpretation is in perfect agreement with reflectivity measurements obtained at 4 K, shown in Fig. 4. The stopband of the DBR is clearly visible and centered at different energies along the two polarization directions, as expected from the sample birefringence.[16] Indeed, below the band gap, n_o is always smaller than n_e in III nitrides.[17] Hence, for a given layer thickness, the stopband is centered at lower energies for $\mathbf{E}\parallel c$, while the magnitude of the shift, in the present case 35 meV, depends on $\Delta n = n_o - n_e$. On top of the stopband the excitonic feature is well resolved for all angles. Its polarization-dependent shift in energy can be clearly identified in the spectral profiles, nearly corresponding to polarization along the optical axes (only small deviations are caused by the angle of incidence of 11°) given in Figs. 4(b) and 4(c).[18] The observed behavior is consistent with PL results obtained at RT [cf. Figs. 3(b) and 3(d)] and confirms the presence of at least two excitonic levels contributing to the optical response. The energy difference between X_{A} and X_{B} amounts to ∼15 meV, which exceeds the value observed in PL experiments [cf. Fig. 3(d)]—an effect which can likely be ascribed to the influence of thermal occupation in luminescence experiments. The value of the energy splitting reveals the contribution of X_{B} to the PL spectra at elevated temperatures reported in Fig. 2(a), which means that the real value of the linewidth of X_{A} at RT

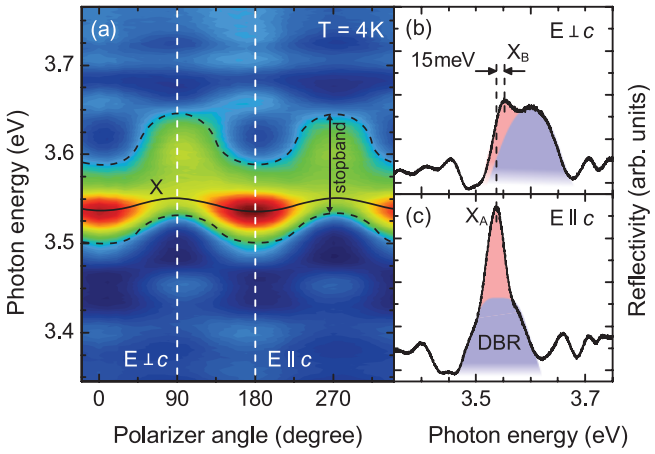

FIG. 4. (Color online) (a) Color map of polarization-resolved reflectivity measurements obtained at 4 K under an angle of 11°. The black solid line marks the position of the excitonic response. Spectra along the white dashed lines are shown on the right-hand side column and nearly correspond to polarization (b) perpendicular and (c) parallel to the c axis. Contributions of excitons and the DBR are highlighted in red (gray) and blue (dark gray), respectively.

might be slightly lower than the one reported in Fig. 2(b). By contrast, the results of Fig. 3(a) should be almost free of the impact of X_B, since the thermal occupation at 4 K is expected to be negligible. Furthermore, it is worth mentioning that there is a better overlap between the DBR stopband and X_A in the extraordinary direction than for X_B in the ordinary one.

IV. INFLUENCE OF STRAIN

Both PL and reflectivity studies indicate a counterpolarization of the QW exciton and the AlGaN barrier with respect to the behavior expected for unstrained GaN and the probed response of the GaN buffer. The latter exhibits a strong linear polarization along $\mathbf{E} \perp c$ and an emission energy of 3.47 eV (see Fig. 3) at 4 K, which matches the expectations for X_A of relaxed GaN.[14,19] At this temperature higher exciton levels are expected to be almost unoccupied. The differing behavior of the AlGaN barrier can be understood if one considers the large negative crystal-field energy in AlN leading to a reversed valence-band ordering and thus a counterpolarized emission with respect to GaN already for low Al contents ($x \sim 9\%$). In this case, the lowest-energy transition B is dominant for $\mathbf{E} \parallel c$.[20]

The discrepancy between the behavior expected for strain-free GaN, and the polarization dependence of the QW emission described above might be related to the compressive strain state of the QWs introduced by the thick AlGaN-based bottom DBR which exhibits smaller lattice constants. To understand the influence of strain, $k \cdot p$ calculations were performed treating an m-plane GaN layer pseudomorphically strained on AlGaN with various x. In other words, it is assumed that the underlying AlGaN layer stack imprints its averaged in-plane lattice constants to the cavity region and therefore to the GaN QWs, leading to a lattice relaxation along the growth direction (m axis) defined by the elastic constants. Here, we used the $k \cdot p$ approach of Chuang and Chang[21] for wurtzite crystals in combination with material constants taken from Refs. 22 and 23. In the following procedure we neglect the variation of the strain state between 4 K and RT due to different thermal expansion coefficients for AlGaN and GaN. This is justified by an expected error $\Delta\epsilon_{mm} \sim 10^{-5}$.[24]

The calculated transition energies displayed in Fig. 5(a) were corrected by a temperature shift of 55 meV obtained from Fig. 2(b), an exciton-binding energy of 41 meV, and a confinement energy of ~40 meV (X_A)—both deduced from envelope function calculations. Note that the effective hole masses along the growth direction for transitions A and B are increased by the strain experienced by the GaN layer, while the electron mass is almost unaffected. As a result, the hole confinement energies are decreased and the reduced effective mass is mainly governed by the electron mass, leading to identical binding energies for X_A and X_B (the probable influence of the anisotropic dielectric constant is neglected here). The position $x = 0$ represents the unstrained case. Increasing the Al content and therefore the compressive in-plane strain causes a blueshift of transition energies, while different deformation potentials and strong p-orbital repulsion lead to the occurrence of anticrossings [Fig. 5(a)] accompanied by an exchange of f_{osc} between $\mathbf{E} \perp c$ and $\mathbf{E} \parallel c$ [Figs. 5(b) and 5(c)]. For $x \sim 5\%$ there is an anticrossing between the B and C bands, and another one appears between the A and B transitions for $x \sim 22\%$. The relative oscillator strengths f^*_{osc} have simply to be multiplied by a material specific constant F to obtain f_{osc} according to Refs. 21,25, and 26:

$$f_{osc} = F \cdot f^*_{osc}. \quad (1)$$

F is a material specific quantity related to Kane's parameter and scales the imaginary part of the refractive index. Within the cubic approximation it is expected to be equal for the two polarization directions.[4] For low strain values ($x < 5\%$) the selection rules undergo only slight changes. In the ordinary direction the optical response is dominated by the lowest-energy transition A, while C rules for $\mathbf{E} \parallel c$. Modifications

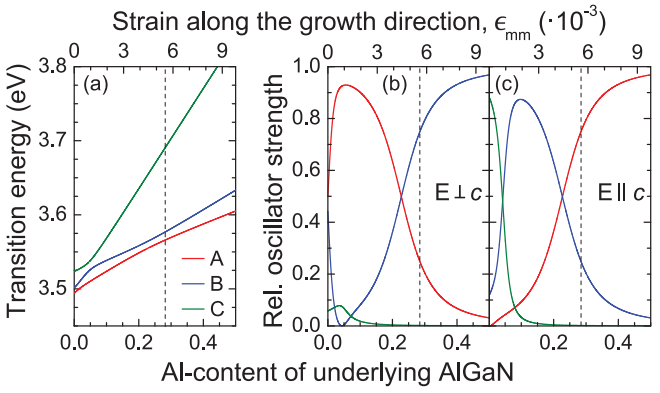

FIG. 5. (Color online) Results of $k \cdot p$ calculations performed for m-plane GaN pseudomorphically strained on AlGaN with varying Al contents (0%–50%). The three graphs contain (a) the evolution of transition energies at the Γ point, and (b),(c) polarization-dependent f^*_{osc} for the interband transitions A, B, and C. The strain state of the QWs deduced from XRD measurements is indicated by the vertical dashed lines.

appear in particular for transition B, which continuously loses influence for $\mathbf{E} \perp c$ while its weight increases for $\mathbf{E} \parallel c$. For higher x the impact of transition C vanishes completely for both polarization directions. Note that due to the anisotropic strain the symmetry between the a and m axes is broken. As a result, f_{osc} are different for the two directions, where $\mathbf{E} \perp c$ ($\mathbf{E} \parallel m$ and $\mathbf{E} \parallel a$) and C is only allowed for polarization $\mathbf{E} \parallel m$ (f_{osc} along this direction are not shown here, because the influence for small angles is negligible). However, for x up to $\sim$22%, transition A still sets the tone for $\mathbf{E} \perp c$, whereas $\mathbf{E} \parallel c$ is now dominated by transition B. Then, with even higher compressive strain an anticrossing between both transitions appears, which is connected with an exchange of f_{osc}. In this regime, the lowest-energy transition A rules the extraordinary direction—the behavior observed in the QWs investigated here.

Complementary high-resolution x-ray diffraction measurements (XRD, not shown here) reveal a fast strain relaxation occurring within the first pairs of the DBR and resulting in intermediate lattice constants corresponding to $x_{\mathrm{XRD}} = 28\%$. This value is close to the geometrical value $x_{\mathrm{geo}} \sim 26\%$ [cf. Eq. (4) hereafter] and is kept over the whole structure, including the cavity section and the QWs. From $k \cdot p$ calculations we therefore expect a transition energy of $\sim$3.56 eV and ρ to be equal to 0.47 for X_{A}. These values are in good agreement with the experimental results: 3.545 eV and $\rho_{\mathrm{PL}} = 0.39$. Consistency with the experiment is also found for the energy difference between A and B excitons: A splitting of 12 meV is deduced from $k \cdot p$ calculations (cf. reflectivity measurements displayed in Fig. 4). Up to a certain extent the minor deviations could be attributed to the slight structural disorder present in the structure, potentially resulting in a lower strain state at this spot position. Note indeed that a strain variation of only 1% is necessary to explain the different ρ values. However, the most probable origin of the small discrepancy might rather be related to the theoretical modeling. In principle, this $k \cdot p$ treatment is exclusively valid for band-to-band transitions occurring in thick layers, i.e., quantum confinement and excitonic effects on f_{osc} are neglected. Nevertheless, it was shown that excitons nearly behave as the bands they belong to[27] and that the influence of quantum confinement is small even for thinner QWs in comparable structures.[28]

V. TUNING THE COUPLING REGIME

From the previous analysis, it appears that the design of the bottom DBR has a strong impact on the optical anisotropy in the structure. Varying the composition of the AlGaN layer pairs (or even switching to AlInN or AlInGaN) allows, on one side, the modification of the birefringence, e.g., the energy position of the stopband center, and, on the other side, the tuning of the distribution of f_{osc} between the different excitons. An effect not discussed so far is the cavity mode energy position in the subsequent full MC, which will also be affected by the birefringence.[10,29] In accordance with the argumentation for the DBR stopband, the cavity mode in the ordinary direction C_o will be blueshifted with respect to the one in the extraordinary direction C_e by $\sim$35 meV.

The coupling strength in a planar anisotropic MC is, for a certain polarization direction y, given by[30]

$$g_y = \hbar \sqrt{\frac{e^2}{2\varepsilon_0 m_0} \frac{N_{\mathrm{QW}}}{n_{C,y}^2 L_{\mathrm{eff}}} f_{\mathrm{osc},y}}, \tag{2}$$

where e, ε_0, and m_0 denote the elementary charge, the vacuum permittivity, and the free electron mass, respectively. N_{QW} corresponds to the number of effectively coupled QWs and L_{eff} to the effective cavity length as defined in Ref. 30. In an ideal system the transition from the weak-coupling regime (WCR), where X and C are the eigenmodes, to the SCR occurs when the coupling strength overcomes the damping rates of the bare modes. In other words, the vacuum Rabi splitting Ω_{VRS}, which corresponds to the splitting between the polariton modes when X and C match in energy, has to exceed zero:[30]

$$\Omega_{\mathrm{VRS},y} = 2 \cdot \mathbf{Re}\left\{ \sqrt{g_y^2 - \frac{\gamma_X^2 + \gamma_C^2}{2}} \right\}. \tag{3}$$

Here, γ_X and γ_C are the homogeneous linewidths of the excitonic transition and the cavity mode, respectively. Considering pseudomorphic growth and keeping the design of the present cavity section, Fig. 6 displays expected Ω_{VRS} values of a complete MC structure as a function of the DBR bilayer compositions x_1 and x_2 for the two polarization directions. As reasonable input parameters, $F = 5.1 \times 10^{13}$ cm^{-2},[31] $N_{\mathrm{QW}} = 16.3$,[32] $\gamma_X = 14$ meV, and $\gamma_C = 10$ meV (Ref. 33) were used. In accordance with Sec. VI and the results reported in Ref. 33, γ_X was extracted from micro-PL measurements performed at 50 K under pulsed excitation. The change in the effective cavity length was taken into account[34] and polarization-dependent f_{osc}^* were extracted from $k \cdot p$ calculations using

$$x_{\mathrm{geo}} = \frac{d_1 x_1 + d_2 x_2}{d_1 + d_2}, \tag{4}$$

where d_1 and d_2 denote the DBR bilayer thicknesses, which are a function of the composition-dependent refractive index at the targeted stopband central wavelength $\lambda_c = 355$ nm.[35] The number of bilayers in the DBR was adjusted to maintain a peak reflectivity of 99.5% and is indicated by the white dashed lines in Fig. 6. Note that for all possible compositions X_{A} remains the lowest-energy transition and X_C was not considered, since it has only a marginal influence for very low values of x_1 and x_2 along the extraordinary direction.

In order to translate this calculation into a predictive phase diagram for the design of realistic structures operating in the WCR or in the SCR (or even in both regimes at the same time), one has to consider nonidealities. In Ref. 13, it was shown both experimentally and theoretically by using the transfer-matrix formalism, that a valid criterion to achieve the SCR should also account for the impact of the inhomogeneous QW linewidth γ_{inh}. When γ_{inh} significantly exceeds Ω_{VRS}, a transition to the WCR occurs, even if Ω_{VRS} is nonzero. Further restrictions are given by the DBR composition: Low Al contents will introduce an additional damping emerging from the AlGaN absorption tail, and a high number of bilayer pairs will likely reduce the surface quality and therefore increase γ_{inh}. The latter might also occur in the region where the required number of pairs is low. Here, the large bilayer composition contrast will result in a

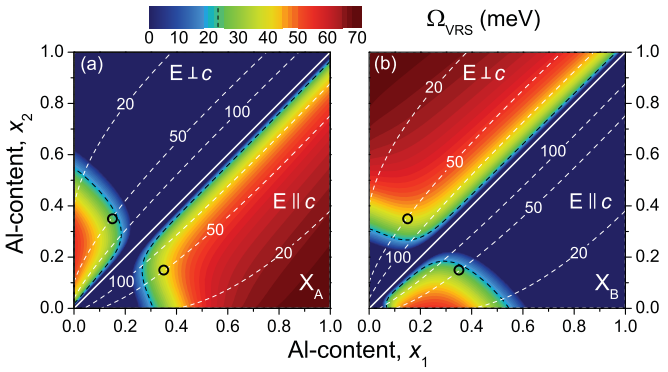

FIG. 6. (Color online) Calculated vacuum Rabi splitting Ω_{VRS} for (a) X_A and (b) X_B as a function of the DBR composition ($Al_{x_1}Ga_{1-x_1}N/Al_{x_2}Ga_{1-x_2}N$). Areas where $x_1 < x_2$ and $x_1 > x_2$ correspond to polarization $\mathbf{E} \perp c$ and $\mathbf{E} \parallel c$, respectively. The number of bilayers (white dashed lines) has been adjusted to keep a 99.5% peak reflectivity. The black dashed lines indicate the case where $\Omega_{VRS} \sim \gamma_{inh}$, and the black open circles mark the position of the present structure.

high strain state, leading to the formation of cracks. Moreover, the overlap between X and the DBR stopband has to be taken into account, since relation (2) is only valid for strong photon confinement.

Under these conditions Fig. 6 discloses the unique opportunity to tune the light-matter coupling regime via strain engineering. For DBRs with a low average Al content ($x_1 + x_2 < 0.35$,) a peculiar situation would occur. According to Fig. 5(b), X_A dominates the ordinary polarization direction and is expected to be in the SCR with C_o, while X_B would be strongly coupled to C_e. In the opposite directions both transitions are expected to be weakly coupled. Assuming C_e is located at lower energy with respect to X_A, in this case the lowest-energy polariton state would be created by the high-energy exciton X_B. This would lead to a crossing of two orthogonally polarized polariton modes at a certain in-plane momentum provided that the DBR matches the modes in both directions. However, the realization of a MC structure based on a very low Al-content DBR will be challenging, since the AlGaN absorption tail will likely lead to a detrimental damping of the photonic component. In the opposite case for a DBR with a high geometrical Al content ($x_1 + x_2 > 0.5$), X_A features the highest f_{osc} for $\mathbf{E} \parallel c$ and will be in SCR along the extraordinary direction, while X_B is expected to be strongly coupled to C_o. In this regime the refractive-index contrast and the resulting crystal quality have to be balanced carefully. The use of bilayer pairs with a high Al-content contrast will lead to plastic relaxation accompanied by an increasing density of crystal defects and thus modify the strain state and affect the inhomogeneous exciton linewidth. With $x_1 + x_2 = 0.5$ for the bottom DBR, the current structure marks the border of the high Al-content regime (open circles in Fig. 6): Both excitons feature an increased degree of linear polarization, i.e., the calculated Ω_{VRS} values for one exciton differ significantly for $\mathbf{E} \parallel c$ and $\mathbf{E} \perp c$, leading to a preferred direction for the SCR. Finally, it is worth mentioning that for an intermediate strain state ($x_1 + x_2 \sim 0.42$ corresponding to $x_{geo} \sim 22\%$) the SCR might take place for both excitons in both crystal directions. This situation has been demonstrated for an organic MC relying on Frenkel excitons in the SCR by Kéna-Cohen and co-workers.[10]

VI. ANISOTROPIC RESPONSE OF THE FULL MICROCAVITY

In this section these theoretical considerations shall be transferred to the full MC structure, which is completed by a dielectric top DBR exhibiting a purely isotropic optical response. Thus, anisotropy arises solely from the nitride layer stack, resulting in the configurations summarized in Figs. 7(c) and 7(d) for $\mathbf{E} \parallel c$ and $\mathbf{E} \perp c$, respectively. Three sources of optical anisotropy have to be considered: the distribution of f_{osc}, the energetic shift of the bottom DBR stopband observed in the half MC, and the differences between C_e and C_o in both energy position and photonic mass in the full MC.[29]

In Fig. 7(a) the far-field emission along the extraordinary direction measured at 50 K is dominated by a dispersive mode converging toward X_A at high angles. We attribute this mode to the lower polariton branch (LPB) emerging from strong coupling between C_e and X_A. The latter features high $f_{osc,e}$ and matches the DBR stopband at low temperatures according to Fig. 4(c). Fitting the dispersion with a two-level coupled oscillator model, we obtain $\Omega_{VRS} = 45$ meV under low injection, in perfect agreement with calculations of Sec. V. The apparent nonthermal LPB occupation results from a relaxation bottleneck due to the high photonic fraction close to zero in-plane momentum.[36] No emission has been detected from the upper polariton branch (UPB), which is commonly observed in large-coupling strength MCs caused by an efficient relaxation, residual damping, and low thermal occupation factors. Along the ordinary direction [Fig. 7(b)] only a weak emission originating from X_A, or to be more

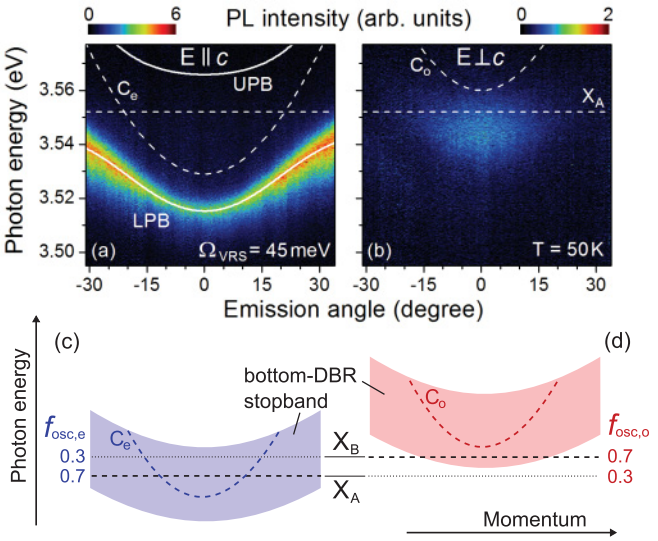

FIG. 7. (Color online) Far-field angle-resolved PL spectra of the complete MC obtained at 50 K along (a) the extraordinary and (b) the ordinary polarization direction. The optical anisotropy created by the nitride layer stack is summarized in (c) and (d) for $\mathbf{E} \parallel c$ and $\mathbf{E} \perp c$, respectively.

precise the superposition of X_A with its localized states, is detected. Indeed, the emission energy is slightly redshifted with respect to the free exciton energy, which is consistent with the occupation of localized states at such low temperatures [cf. Figs. 2(a) and 3(c), and corresponding explanations] and the low excitation level. The cavity mode located at higher energy becomes only visible in the high excitation regime. This effect and the nonlinear emission properties, including a detailed discussion of the full MC, will be published elsewhere.[33] However, the presence of the uncoupled modes is a clear signature of the WCR for $\mathbf{E} \perp c$ created by the low $f_{\mathrm{osc},o}$ for X_A and its decreased overlap with the DBR stopband.

Despite the fact that the thermal occupation and thus the PL contribution of X_B is expected to be almost negligible in the low injection regime at 50 K (cf. Figs. 3 and 4), the coupling regime prediction for X_B is more difficult. Note that the energy splitting between X_A and X_B is comparable to the value of the inhomogeneous broadening present in the sample, preventing a completely independent treatment of the two excitonic transitions. However, when considering the theoretical results of Fig. 6, X_B is expected to be weakly coupled to C_e, while $f^{B}_{\mathrm{osc},o}$ should be sufficient to reach the SCR for $\mathbf{E} \perp c$. Nevertheless, in PL and reflectivity (not shown here) studies no indication of any anticrossing has been observed along the ordinary direction, which is likely caused by the location of X_B close to the lower stopband edge [cf. Figs. 4(b) and 7(d)], leading to a detrimentally decreased coupling strength and thus to the appearance of the WCR.

VII. CONCLUSION

In conclusion, a high-quality m-plane GaN/AlGaN MQW structure intended to be the active region of a planar MC was grown on top of an AlGaN-based DBR using nonpolar bulk GaN as the substrate. The QWs experience highly compressive strain induced by the underlying layer stack, resulting in a reversed polarization behavior with respect to unstrained GaN. Reflectivity and PL studies are in excellent agreement with $k \cdot p$ calculations and indicate the possibility to tune the nature of the light-matter coupling in anisotropic microcavities by managing the strain state of the QWs. Modifying the Al content of the bottom DBR allows to bring the different excitons into the strong- or weak-coupling regime with the two orthogonal cavity modes. Owing to the anisotropy of the nitride layer stack and in agreement with theoretical considerations, the complete MC structure shows a polarization-dependent coupling regime, i.e., weak- and strong-coupling regimes coexist along orthogonal polarization planes.

ACKNOWLEDGMENTS

This work was supported by the NCCR Quantum Photonics, research instrument of the Swiss National Science Foundation (SNSF), by the SNSF (Grant No. 200020-113542), by the EU-project Clermont4 (Grant No. FP7-235114), by the European Regional Development Fund (Grant Innovative Economy POIG.01.01.02-00-008/08), and the Polish Ministry of Science and Higher Education (Project No. N-N202-010134). We are grateful to J. Domagala for XRD measurements.

*georg.rossbach@epfl.ch
†Now at CEA-LETI, Minatec Campus, 38054 Grenoble, France.

[1] M. Leroux, N. Grandjean, M. Läugt, J. Massies, B. Gil, P. Lefebvre, and P. Bigenwald, Phys. Rev. B **58**, 13371 (1998).
[2] P. Waltereit, O. Brandt, A. Trampert, H. T. Grahn, J. Menniger, M. Ramsteiner, M. Reiche, and K. H. Ploog, Nature (London) **406**, 865 (2000).
[3] K. Shimada, T. Sota, and K. Suzuki, J. Appl. Phys. **84**, 4951 (1998).
[4] M. Suzuki, T. Uenoyama, and A. Yanase, Phys. Rev. B **52**, 8132 (1995).
[5] G. Christmann, R. Butté, E. Feltin, A. Mouti, P. A. Stadelmann, A. Castiglia, J.-F. Carlin, and N. Grandjean, Phys. Rev. B **77**, 085310 (2008).
[6] C. Weisbuch, M. Nishioka, A. Ishikawa, and Y. Arakawa, Phys. Rev. Lett. **69**, 3314 (1992).
[7] A. Imamoglu, R. J. Ram, S. Pau, and Y. Yamamoto, Phys. Rev. A **53**, 4250 (1996).
[8] S. Christopoulos, G. Baldassarri Höger von Högersthal, A. J. D. Grundy, P. G. Lagoudakis, A. V. Kavokin, J. J. Baumberg, G. Christmann, R. Butté, E. Feltin, J.-F. Carlin, and N. Grandjean, Phys. Rev. Lett. **98**, 126405 (2007).
[9] G. Christmann, R. Butté, E. Feltin, J.-F. Carlin, and N. Grandjean, Appl. Phys. Lett. **93**, 051102 (2008).
[10] S. Kéna-Cohen, M. Davanço, and S. R. Forrest, Phys. Rev. Lett. **101**, 116401 (2008).
[11] S. Ghosh, P. Misra, H. T. Grahn, B. Imer, S. Nakamura, S. P. DenBaars, and J. S. Speck, J. Appl. Phys. **98**, 026105 (2005).
[12] P. Corfdir, P. Lefebvre, J. Levrat, A. Dussaigne, J.-D. Ganière, D. Martin, J. Ristić, T. Zhu, N. Grandjean, and B. Deveaud-Plédran, J. Appl. Phys. **105**, 043102 (2009).
[13] G. Christmann, R. Butté, E. Feltin, J.-F. Carlin, and N. Grandjean, Phys. Rev. B **73**, 153305 (2006).
[14] P. Misra, O. Brandt, H. T. Grahn, H. Teisseyre, M. Siekacz, C. Skierbiszewski, and B. Lucznik, Appl. Phys. Lett. **91**, 141903 (2007).
[15] Y. J. Sun, O. Brandt, M. Ramsteiner, H. T. Grahn, and K. H. Ploog, Appl. Phys. Lett. **82**, 3850 (2003).
[16] D. M. Schaadt, O. Brandt, S. Ghosh, T. Flissikowski, U. Jahn, and H. T. Grahn, Appl. Phys. Lett. **90**, 231117 (2007).
[17] S. Shokhovets, R. Goldhahn, G. Gobsch, S. Piekh, R. Lantier, A. Rizzi, V. Lebedev, and W. Richter, J. Appl. Phys. **94**, 307 (2003).
[18] Due to the complexity of the structure and the uncertainty on the optical constants of each layer, the exact position of the QW excitons cannot be modeled in the reflectivity spectra. Nevertheless, the features assigned to the excitons in Fig. 4(a) were found to be free of any PL contribution and nondispersive in angle-resolved measurements. Even if the absolute positions of the QW excitons cannot be extracted from the present data, the polarization-dependent shift in energy is revealed.
[19] K. Kornitzer, T. Ebner, K. Thonke, R. Sauer, C. Kirchner, V. Schwegler, M. Kamp, M. Leszczynski, I. Grzegory, and S. Porowski, Phys. Rev. B **60**, 1471 (1999).

[20]G. Rossbach, M. Feneberg, M. Röppischer, C. Werner, N. Esser, C. Cobet, T. Meisch, K. Thonke, A. Dadgar, J. Bläsing, A. Krost, and R. Goldhahn, Phys. Rev. B **83**, 195202 (2011).
[21]S. L. Chuang and C. S. Chang, Phys. Rev. B **54**, 2491 (1996).
[22]I. Vurgaftman and J. R. Meyer, J. Appl. Phys. **94**, 3675 (2003).
[23]S. Ghosh, P. Waltereit, O. Brandt, H. T. Grahn, and K. H. Ploog, Phys. Rev. B **65**, 075202 (2002).
[24]H. Iwanaga, A. Kunishige, and S. Takeuchi, J. Mater. Sci. **35**, 2451 (2000).
[25]Y. M. Sirenko, J. B. Jeon, B. C. Lee, K. W. Kim, M. A. Littlejohn, M. A. Stroscio, and G. J. Iafrate, Phys. Rev. B **55**, 4360 (1997).
[26]S. Shokhovets, O. Ambacher, B. K. Meyer, and G. Gobsch, Phys. Rev. B **78**, 035207 (2008).
[27]B. Gil and O. Briot, Phys. Rev. B **55**, 2530 (1997).
[28]R. Mata, A. Cros, J. A. Budagosky, A. Molina-Sánchez, N. Garro, A. García-Cristóbal, J. Renard, S. Founta, B. Gayral, E. Bellet-Amalric, C. Bougerol, and B. Daudin, Phys. Rev. B **82**, 125405 (2010).
[29]T. Zhu, A. Dussaigne, G. Christmann, C. Pinquier, E. Feltin, D. Martin, R. Butté, and N. Grandjean, Appl. Phys. Lett. **92**, 061114 (2008).
[30]V. Savona, L. C. Andreani, P. Schwendimann, and A. Quattropani, Solid State Commun. **93**, 773 (1995).
[31]This value was obtained for thinner *c* plane QWs in Ref. 5. The use of this value is justified by the partial compensation between the decreasing f_{osc} due to the QCSE and the effect of the higher quantum confinement.
[32]The number of effectively coupled QWs, N_{QW}, is reduced with respect to the geometrical one, because of the decreased overlap between the electric field intensity and the QWs located slightly apart from the field antinodes as calculated in Ref. 30.
[33]J. Levrat, G. Rossbach, A. Dussaigne, H. Teisseyre, G. Cosendey, M. Glauser, M. Cobet, M. Bockowski, I. Grzegory, T. Suski, R. Butté, and N. Grandjean (unpublished).
[34]Owing to the lack of experimental values for the extraordinary refractive index in the AlGaN system, L_{eff} was derived for both polarization directions as defined in Ref. 30 using the optical constants of the ordinary dielectric function given in Ref. 35. The error created by the differing refractive-index contrast in the bilayers along the two optical axes is marginal (cf. Ref. 26).
[35]D. Brunner, H. Angerer, E. Bustarret, F. Freudenberg, R. Höpler, R. Dimitrov, O. Ambacher, and M. Stutzmann, J. Appl. Phys. **82**, 5090 (1997).
[36]F. Tassone and Y. Yamamoto, Phys. Rev. B **59**, 10830 (1999).